CONFERENCE PRE-PRINT

GYROKINETIC LINEAR SIMULATION OF HOT-ION MODE IN GLOBUS-M2 SPHERICAL TOKAMAK

E.O. KISELEV, G.S. KURSKIEV, V.B. MINAEV, N.V. SAKHAROV, V.K. GUSEV, M.I. PATROV, Y.V. PETROV, I.M. BALACHENKOV, N.N. BAKHAREV, V.I. VARFOLMEEV, N.S. ZHILTSOV, I.V. MIROSHNIKOV, O.M. SKREKEL, V.V. SOLOKHA, A.YU. TELNOVA, E.E. TKACHENKO, V.A. TOKAREV, S.YU. TOLSTYAKOV, E.A. TUKHMENEVA, K.D. SHULYATIEV, P.B. SHCHEGOLEV

Ioffe Institute
St. Petersburg, Russian Federation
Email: nightkeo@gmail.ru

A.M. PONOMARENKO, A.Y. YASHIN
Peter the Great St. Petersburg Polytechnic University
St. Petersburg, Russian Federation

Abstract

The experimental results in Globus-M2 spherical tokamak hot ion mode discharges with power injected by the NBI system with hydrogen and deuterium beam show increased ion heat transport when heavier isotopes are considered, thus moving from H to D beam. In order to characterize the turbulence behavior, these discharges are studied in detail and interpreted with gyrokinetic linear simulations. For the plasma condition in hydrogen beam experiment, TEM mode is responsible for most of the ion heat transport. But in deuterium beam shot ion heat transport is near neoclassical level, unstable ITG mode is suppressed by ExB rotational shear.

1. INTRODUCTION

In experiments on plasma heating in H-mode at spherical tokamaks (ST) with a toroidal magnetic field B_T<0.55 T, it was found that ion heat transport is well described by neoclassical theory [1] [2]. Subsequent experiments on compact ST with higher magnetic field B_T=0.9 T demonstrated the possibility of achieving sub-fusion temperatures near 4–8 keV [3][4][5] using neutral beam injection. A more detailed analysis showed that the maximum achievable ion temperature depends primarily on the mass of the injected beam atoms. In order to characterize the turbulence dependence on the isotope mass, these discharges are studied in detail and interpreted with gyrokinetic linear simulations.

2. EXPERIMENTAL RESULTS

Let’s compare 2 similar Globus-M2 shots in hot ion mode - #42777 and #42119 (Table 1) [6], with plasma current I_p=350 kA, toroidal magnetic field B_T=0.9 T, electron plasma density $<n_e>=3.7\ 10^{19}\ m^{-3}$ and with neutral beam injection. One shot with hydrogen beam - #42119, injection power P_{inj}=1.35 MW and one with less power P_{inj}=1.15 MW and with deuterium beam - #42777. In both discharges the plasma is deuterium-based, but injection of different isotopes leads to a change in the average main ion mass: in the deuterium discharge, the hydrogen-to-deuterium density ratio is n_H/n_D=0.25, and the average mass number of the main ion is m_i=1.8 a.m.u. Meanwhile, in the hydrogen discharge the density ratio is 2.6 times higher— n_H/n_D=0.66, which results in a slight decrease of the average mass number of the main ion to m_i = 1.6 a.m.u. Electron temperature is practically the same with central temperature near T_{e0}=1.5 keV. But ion temperature has major differences: in shot #42777 with deuterium beam ion temperature is higher, near 4 keV, but in shot with hydrogen beam #42119 ion temperature is lower, near 2.5 keV. Energy confinement time in deuterium shot is 2 times higher (12-16.5 ms, and succeed IPB98(y,2) scaling in 2 times), in comparison with hydrogen beam discharge, mostly due to the increased ion energy content and slightly lower NBI power. Electron heat transport is dominated and mostly anomalous in both shots. In deuterium shot ion heat conductivity is very close to values, predicted by neoclassical theory, anomalous ion heat transport near zero. But in hydrogen beam discharge ion heat conductivity is 3 times higher, than neoclassical prediction, anomalous ion heat transport is significant.

TABLE 1. Power balance analysis of discharges with hydrogen and deuterium beam

	#42119 (H->D)	#42777 (D->D)
W_e, *kJ*	4.4	4.6
W_i, *kJ*	4.1	7.1
W_{th}, *kJ*	8.5	11.7
$P_{NBI,abs}$, *kW*	850-1150	540-810
$P_{NBI,i}$, *kW*	435-640	390-590
$P_{NBI,e}$, *kW*	380-510	150-220
t_E, *ms*	8.4-6.3	16.5-12
$\tau_{E,i}$, *ms*	15-8.5	80-24
$\tau_{E,e}$, *ms*	6-5	7.6-6.8
χ_e, m^2/s	1.2-1	1.3-1
χ_i, m^2/s	2.7-3.7	0.3-0.95
$\chi_{i,neo}$, m^2/s	~1	~1
P_{ie}, *kW*	160	300
Z_{eff}	3.5	3
P_{oh}, *kW*	200	170

3. GYROKINETIC ANALYSIS

Micro-turbulence is considered to be a major candidate in driving anomalous transport in fusion plasmas [7]. The long wavelength (ion-scale) ion temperature gradient (ITG) mode [8], trapped electron mode (TEM) [9], kinetic ballooning modes (KBMs) [9], micro-tearing (MT) [11][12][13] mode and the short-wavelength (electron-scale) electron temperature gradient (ETG) mode [14][15] are well-known instabilities which could drive micro-turbulence in fusion plasmas. And understanding of microinstabilities behavior is key factor for understanding experiments on Globus-M2.

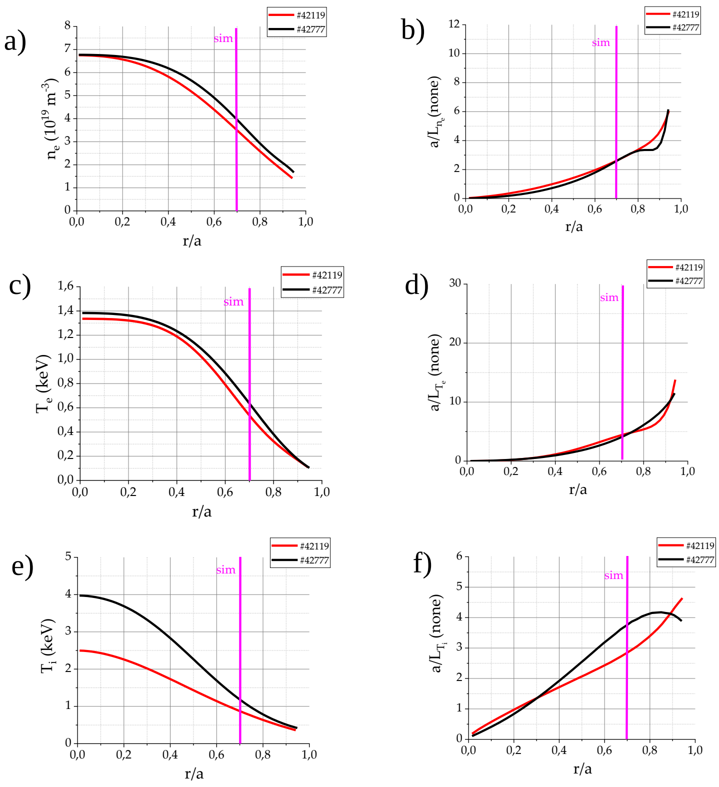

Fig. 1. Fits to the measured temperature and density profiles and the normalized temperature and density gradients for electron and ions for discharges with hydrogen and deuterium beam.

3.1. Input data

Firstly, we discuss about input data for gyrokinetic simulation. These shots have intensive sawtooth oscillations in core region with normalized minor radius lower than r/a<0.6. Gyrokinetic simulation in core region is meaningless because of MHD instabilities and it was performed in gradient region with r/a=0.7.

Profiles of electron and ion temperature, electron density etc, were measured with the diagnostics described in [6]. Fits to the temperature and density profiles and the turbulence drive terms, the normalized temperature and density gradients, are shown in Fig. 1. Fits to the full set of measured profile data and other inputs were used by the ASTRA [16] code to solve the power balance equations. All inputs for gyrokinetic simulations that describe the plasma geometry and profile parameters are derived from the ASTRA output.

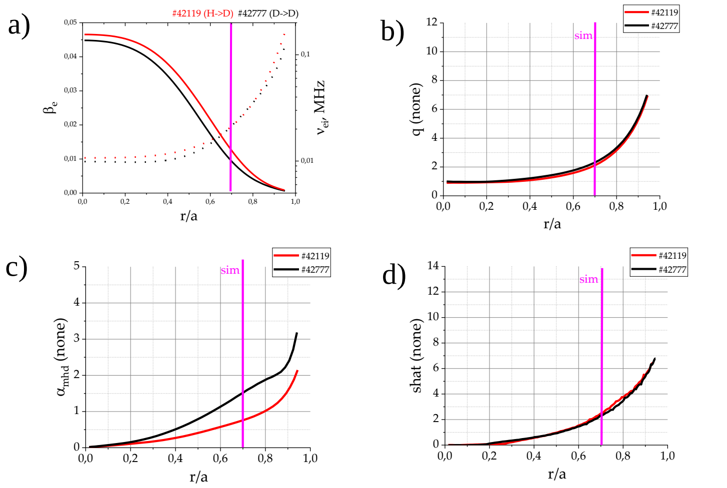

Fig. 2. Additional quantities, that can be responsible for turbulence destabilization: electron beta β_e, ν_{ei} electron ion collisional frequency, α_{mhd} which reflects the Shafranov shift effects on the shape of magnetic surfaces, safety factor q and magnetic shear $\hat{s}$.

One of the main sources of microinstabilities destabilization in tokamak plasmas is the normalized profile gradients a/L_X:

$$^{a}/_{L_X} = -\frac{a}{X}\frac{dX}{dr} \quad (1)$$

with a – minor radius of plasma, r – minor radius of magnetic surface and profiles $X \in \{T_e, T_i, n_e, n_i, n_{imp}\}$ for electron, ion, impurity temperature and density, consequently. The considered discharges with hydrogen and deuterium injection, the electron temperature and density profiles, as well as their gradients, are almost identical (Fig. 1a,b,c,d). However, the ion temperature in the center of the deuterium discharge is 1.6 times higher than in the hydrogen discharge, which leads to a significant change in the ion temperature gradient: in the deuterium discharge, a/L_{T_i}=3.8, while in the hydrogen discharge it is 1.3 times lower — a/L_{T_i} = 2.9 (Fig. 1e,f).

The differences in ion temperature lead to an increased plasma kinetic pressure in the center of the deuterium discharge, which is 1.6 times higher than in the hydrogen discharge. However, the change in pressure hardly affects the shape of the magnetic surfaces or the safety factor, which in both discharges is q = 1.67 (Fig. 2c), as well as the magnetic shear (Fig. 2c), $\hat{s} = \frac{r}{q}\frac{dq}{dr} = 2.2$ (where r is the minor radius of the magnetic surface). At the same time, the parameter α_{mhd} (Fig. 2d), which reflects the Shafranov shift effects on the shape of magnetic surfaces:

$$\alpha_{mhd} = -q^2 R \frac{d\beta}{dr} \quad (2)$$

where $\beta = \beta_e + \beta_i$, differs much more significantly. For the discharge with deuterium injection α_{mhd} =1.5, while for the hydrogen discharge it is twice as small — 0.75.

Additionally, electron beta can be responsible for turbulence destabilization (Fig. 2a):

$$\beta_e = \frac{8\pi n_e T_e}{B_T^2} \quad (3)$$

which is 0.9% for the hydrogen-injection discharge and slightly higher, 1.3%, for the deuterium discharge. Another important parameter is the electron–ion collision frequency ν_{ei} (in CGS units) on Fig 2a:

$$\nu_{ei}\frac{a}{c_s} = \frac{\pi Z^2 e^4 n_i \ln\Lambda}{2 m_e^{\frac{1}{2}} T_e^{\frac{3}{2}}}\frac{a}{c_s} \quad (4)$$

where $\ln\Lambda$ is the Coulomb logarithm, m_e is the electron mass, e is the electron charge, and Z is the charge of the main plasma ion. ν_{ei} is normalized on minor radius a and sound speed $c_s = \sqrt{T_e/m_i}$ relation. This quantity varies significantly with the normalized minor radius; therefore, differences of nearly 1.5 times after normalization are negligible.

And also, there is differences in effective charge, that was measured by Bermshtrahlung radiation power diagnostic, in hydrogen shots Z_{eff}=3.5, deuterium shot Z_{eff} =3. In the discharge with hydrogen injection, a more powerful beam was used, which leads to wall sputtering. In addition, hydrogen has a higher velocity at the same beam energy and sputters the wall more effectively than deuterium.

Finally, the quantities whose differences between discharges can significantly affect the results of gyrokinetic analysis include the ion temperature gradient a/L_{Ti}, the effective charge Z_{eff}, and α_{MHD}. A summary of the input data for the gyrokinetic analysis is presented in Table 2.

TABLE 2 Input parameters for gyrokinetic simulations

r/a=0.7	#42119 H->D	#42777 D->D
a, m	0.235	0.224
q	1.67	1.67
s	2.26	2.18
α_{mhd}	0.75	1.5
a/L_{Te}	4.5	4.08
a/L_{Ti}	2.9	3.8
a/L_{ne}	2.65	2.59
Z_{eff}	3.5	3
β_e, %	0.9	1.3
$\nu_{ei}(a/c_s)$	0.84	0.53

3.2. Settings for gyrokinetic simulations

The turbulent transport inside the plasma when moving from H to D beam in the Globus-M2 device is investigated by means of gyrokinetic linear simulation, that was performed with the GENE code [17] in the flux-tube linear approximation mode. The unperturbed plasma distribution function was assumed to be Maxwellian. All electromagnetic effects were included in the model: the perpendicular and parallel magnetic fluctuations were considered. According to the δf method, the distribution function was represented as a sum of the static Maxwellian background F_0 function and the small fluctuating part f_1. Three particle species were considered by default: electrons, thermal deuterium ions and carbon ions. Collisions are modeled using the linearized Landau-Boltzmann operator. The magnetic geometry fits the analytical Miller form [18].

3.3. Results of gyrokinetic simulations

As a result of local linear simulations in the gradient region at r⁄a = 0.7, the dependence of the growth rate of microinstabilities on the wavenumber was obtained (Fig. 3). For better comparison of data from different experiments, the results are presented in absolute values.

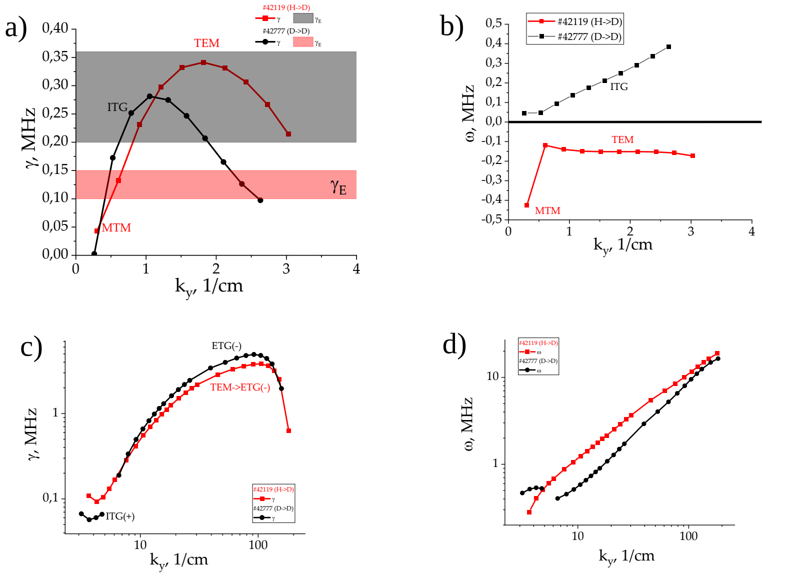

Fig. 3. Gyrokinetic calculation results and the dependence of the growth rate and frequency of microinstabilities on the wavenumber in absolute values for long-wavelength (ion scale) – a,b and for short-wavelength (electron scale) – c,d. ExB rotational shear is indicated by dark (for D-beam shot $\gamma_{E,WM}$=0.08-0.15 MHz) and red (for H-beam shot $\gamma_{E,WM}$=0.2-0.4 MHz) bands in plot a. Maximum growth rate of ITG is near ExB rotational shear, but for TEM maximum growth rate is significantly higher, than ExB shear.

It was found that in the discharge with hydrogen injection (#42119), the TEM instability (ion scale trapped electron mode, characterized by negative frequency, according to electron diamagnetic drift direction) dominates at long wavelengths (ion scale). Maximum growth rate is 0.34 MHz near k_y=1.8 cm^{-1}. In contrast, in the deuterium injection experiment (#42777) at the same normalized minor radius r⁄a = 0.7 at long-wavelengths, the ITG instability (ion temperature gradient mode, with positive frequency, according to ion diamagnetic drift direction on ion scale) is unstable. Maximum growth rate is 0.28 MHz near k_y=1.05 cm^{-1}. The results are presented in Fig. 3a, 3b. While in the short-wavelength microturbulence region (electron scale), the ETG mode is unstable, identified by the negative frequencies associated with the electron diamagnetic drift direction (Fig. 3c and 3d).

The above results were obtained using gyrokinetic linear modeling, which does not allow for determining the absolute values of turbulent heat fluxes. For this purpose, nonlinear simulation must be carried out. However, the obtained data will be used later to explain the experimental results. It is not clear how the heat fluxes found with nonlinear ion-scale and electron-scale simulations contribute to the collective heat flux. Generally, multi-scale simulations that simultaneously resolve both scale ranges are necessary to answer this question. But these simulations are very expensive. A heuristic rule has emerged from pioneering work [21][22][23][24] using a reduced mass ratio ($\sqrt{m_i/m_e} = 20$) and $\hat{s} - \alpha$ geometry, with $\alpha = 0$. Namely, if the ratio of maximum growth rates at the electron and ion scales is much larger than the square root of the mass ratio [25],

$$\gamma^{max}_{high\,k_y}/\gamma^{max}_{low\,k_y} \gg \sqrt{m_i/m_e} \tag{5}$$

then multi-scale effects could be present. This is because the contributions by the electron-scale turbulence to the overall heat transport could be important. Otherwise, turbulent structures at the ion scales disrupt the efficient heat transport at the electron scales. In our case the mass ratio is $\sqrt{m_i/m_e} = 57$ for D-beam shot, and $\sqrt{m_i/m_e} = 54$ for H-beam shot. The ratio between the maximum growth rates for deuterium beam discharge is $\gamma^{max}_{ETG}/\gamma^{max}_{ITG} = 17.7$ and for hydrogen beam shot is $\gamma^{max}_{ETG}/\gamma^{max}_{TEM} = 11.2$. Therefore, our linear simulations with the nominal experimental parameters indicate that multiscale effects could not be present.

More recently, a model for saturation of multi-scale turbulence by zonal flow mixing has been proposed [26]. In this model, an important parameter is the RMS velocity of zonal flows (V_{ZF}), which saturates at $V_{ZF} = Max(\gamma/k_y)$, where γ is the linear growth rate of a turbulent mode with wavenumber k_y. According to this model, multi-scale effects could be present when

$$Max\left(\gamma_{high\,k_y}/k_y\right) \geq Max\left(\gamma_{low\,k_y}/k_y\right). \tag{6}$$

This criterion has been validated on recent multiscale simulations using realistic mass ratio and geometry [23,24]. For our linear simulations of deuterium beam discharge with unstable ITG mode $Max(\gamma_{ETG}/k_y) = 5.3\,10^4\ cm/s$, $Max(\gamma_{ITG}/k_y) = 8.5\,10^5\ cm/s$ this criterion is not satisfied. The same for hydrogen beam discharge: $Max(\gamma_{ETG}/k_y) = 3.6\,10^4\ cm/s$, $Max(\gamma_{ITG}/k_y) = 1.9\,10^5\ cm/s$.

In summary, linear simulations for D-beam shot identify coexisting ITG and ETG modes and for H-beam – TEM and ETG. But this modes in both cases could not engage in multi-scale interactions. Further discussion will focus on long-wavelength modes.

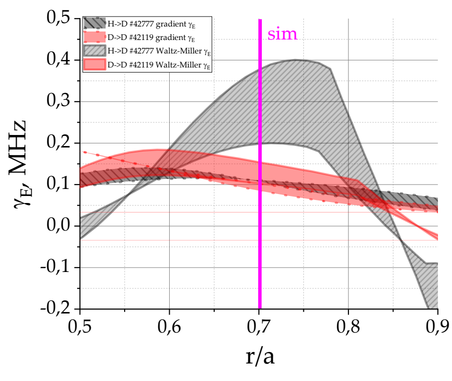

Fig. 4. The dependence of rotational shear on normalized minor radius by simple formula as gradient and by Waltz-Miller formula. Hydrogen beam discharge - the rotational shear calculated using the Waltz-Miller formula and formula (1) are almost equal - $\gamma_{E,WM}$=0.08-0.15 MHz. Deuterium beam discharge, the Waltz-Miller shear is significantly higher by 0.1-0.3 MHz compared to formula (1), $\gamma_{E,WM}$=0.2-0.4 MHz.

It should also be noted that all the gyrokinetic calculations presented here were performed in initial-value mode; therefore, the microturbulence calculations show the fastest-growing mode. Additionally, GENE simulations were performed with eigenvalue solver using the SLEPC/PETSC libraries. As a result, no sub-modes were identified.

3.4. Rotational shear

An important role in the behavior of microinstabilities is played by the E×B shear, which arises due to the torque generated by neutral beam injection. If the growth rate of the instability becomes smaller than the shear, the instability is suppressed or partially suppressed. The E×B shear is calculated using the Waltz-Miller formula $\gamma_{E,WM}$ [19] and by simple formulae, just as a gradient of rotational frequency $\gamma_{E,grad}$:

$$\gamma_{E,WM} = -\frac{r}{q} \cdot \frac{d\left(E_R/B_pR\right)}{dr} \tag{7}$$

$$E_R = \frac{1}{eZ_in_i}\frac{dp_i}{dr} + B_pV_{tor} - B_TV_p \tag{8}$$

$$\gamma_{E,grad} = \frac{r}{q} \cdot \frac{d\omega_{tor}}{dr} \tag{9}$$

where E_R radial electric field by neoclassical formulae, r – local minor radius, q – safety factor, B_p – poloidal magnetic field, B_T – toroidal magnetic field, R – major radius, V_{tor} – toroidal velocity, ω_{tor} – toroidal frequency, V_p – poloidal velocity by neoclassical formulae by ASTRA+NCLASS [20], Z_i – main ion charge, e – electron charge, ion pressure $p_i = n_iT_i$ by multiplying ion density n_i and ion temperature T_i.

E×B shear for both shots is presented in Fig. 4. Since the calculation of shear using the Waltz-Miller formula involves the gradient of the radial electric field, i.e., the second derivative of ion temperature, the calculation error is high. For the hydrogen discharge, the rotational shear calculated using the Waltz-Miller formula and formula (9) are slightly different from each other within the gradient calculation error and reach values of 0.08-0.15 MHz. However, for the deuterium discharge, the Waltz-Miller shear is significantly higher by 0.1-0.3 MHz compared to formula (1), reaching values of 0.2-0.4 MHz.

Maximum growth rate of TEM mode for H-beam discharge is γ = 0.34 MHz (Fig. 3a), which is significantly higher than E×B shear γ_E = 0.08-0.15 MHz. For this reason, in this discharge enhanced electron and ion transport driven by the TEM mode is observed. But in shot with deuterium injection case performed under nearly identical conditions, the ion heat transport is close to the value predicted by neoclassical theory. In that case, the E×B shear is γ_E = 0.2-0.4 MHz, which is nearly equal to the maximum growth rate of the ITG mode, γ = 0.28 MHz (Fig. 3a). Consequently, short-wavelength microinstabilities in the deuterium injection discharge are almost completely suppressed.

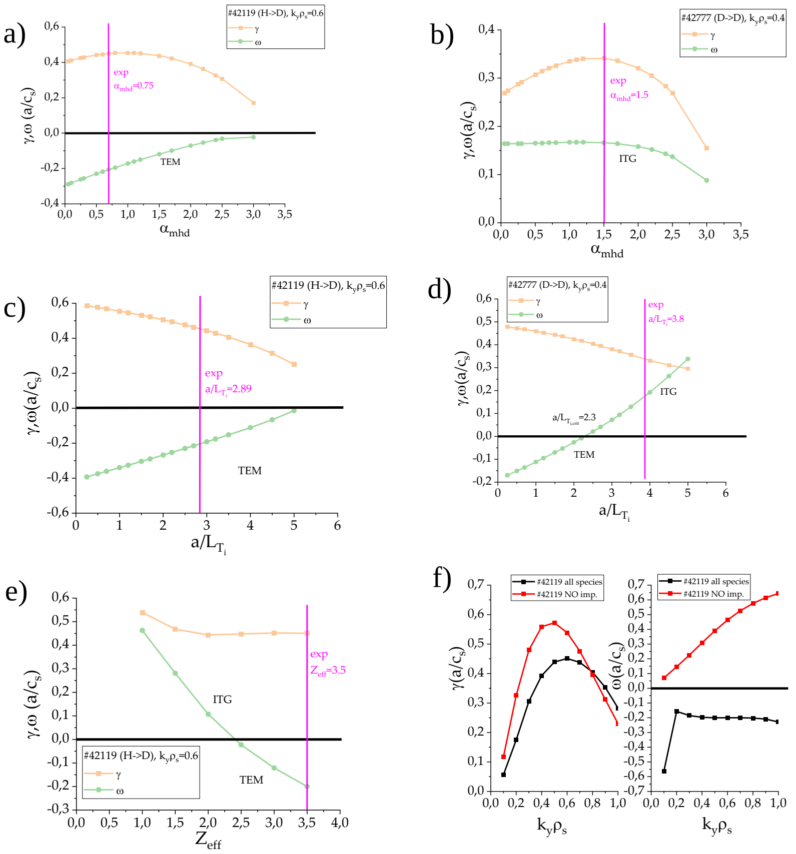

Fig. 5. Parameters scan for with wavevector with maximum growth rate of α_{mhd} – a and b for H and D-beam shot, ion temperature gradient a/L_{Ti} – c, d for H and D-beam shot, and Z_{eff} scan – e for normalized wave vector $k_y\rho_s$=0.6, f – comparing wavevector scan with calculation without impurities for H-beam shot.

3.5. Sources of ITG and TEM destabilization

This chapter is devoted to find the source of ITG and TEM destabilization in these very similar shots. In further gyrokinetic calculations and scans, all the input data was fixed, and some parameters were changed to find the main factor of ITG and TEM mode destabilization. There are 3 parameters with significant differences: α_{mhd}, Z_{eff}, a/L_{Ti}. First factor is α_{mhd} and there is no evidence of turbulence type transition, this parameter is responsible only for level of growth rate – Fig. 5 a,b. Ion temperature gradient scan in hydrogen shot is shown that TEM mode is stabilized with $a/L_{Ti,crit}$=5, but $a/L_{Ti,exp}$=2.9 (Fig. 5c). ITG mode in deuterium beam shot is unstabilized with a/L_{Ti}=2.3 ($a/L_{Ti,exp}$=3.8) – Fig. 5d. We can conclude that ion temperature gradient one is of the main factor for ITG destabilization, but in case of hydrogen beam shot a/L_{Ti} is not. And second important factor is effective charge. In the simulation of hydrogen beam shot without impurities TEM mode is suppressed, and ITG mode in unstabilized – Fig. 5f. But with increased effective charge linear growth rate decrease, ITG mode is suppressed and TEM mode destabilized – Fig 5e. We can conclude, that main factors for TEM destabilization is decreased ion temperature gradient and increased Z_{eff}.

4. CONCLUSION

In experiments on plasma heating with deuterium beam on Globus-M2 with plasma current I_p=350 kA, toroidal magnetic field B_T=0.9 T, electron plasma density $\langle n_e \rangle$=3.7 10^{19} m^{-3} it was found that ion heat transport is well described by neoclassical theory. Meanwhile, in the hydrogen beam discharge with slightly more powerful NBI ion heat transport is anomalous. Energy confinement time in deuterium shot is 2 times higher (12-16.5 ms), in comparison with hydrogen beam discharge. In order to characterize the turbulence, these discharges are studied in detail and interpreted with gyrokinetic linear simulations.

In experiment #42777 with deuterium injection, the ITG mode is unstable, but in discharge #42119 with hydrogen injection, the TEM mode is unstable. The primary factor unstabilizing ITG mode in the deuterium beam discharge is increased ion temperature gradient, with a/L_{Ti} = 3.8 compared to 2.9 in the hydrogen beam discharge, as well as a lower effective charge: Z_{eff} = 3 versus 3.5 in H-beam. ETG mode is unstable in both discharges.

Both types of instabilities (ITG and TEM) can generate anomalous heat flux in both electrons and ion channels. But nonlinear simulation must be carried out for calculations of turbulence contribution to overall heat flux. It is not clear how the heat fluxes found with nonlinear ion-scale and electron-scale simulations contribute to the collective heat flux. Generally, multi-scale simulations that simultaneously resolve both scale ranges are necessary to answer this question. But these simulations are very expensive.

The simple criterion of multi-scale effects was used on the base of linear simulation results and on the base of the heuristic rule (5), and second criterion was based on the model for saturation of multi-scale turbulence by zonal flow mixing (6). Therefore, our linear simulations with the nominal experimental parameters indicate that multiscale effects could not be present and turbulent heat fluxes are associated with ion-scale instabilities only.

And an important role in the behavior of micro-instabilities is played by the E×B rotational shear. If the growth rate of the instability becomes smaller than the rotational shear, this instability gets suppressed or partially suppressed. Such a situation occurs in the discharge with deuterium injection, where the rotational shear γ_E = 0.2-0.4 MHz. This value at the same level as the maximum growth rate of the ITG mode, which is 0.28 MHz and ITG is almost stabilized, anomalous ion heat transport is decreased, and negligible in comparing with neoclassical losses. In the discharge with hydrogen injection, γ_E = 0.08-0.15 MHz, which is significantly lower than the maximum growth rate of the TEM mode, which is 0.34 MHz. In this case, anomalous ion transport is dominated. Thus, the power balance calculations are in consistent with the gyrokinetic simulation.

ACKNOWLEDGEMENTS

The work was performed using equipment owned by the Federal Joint Research Center "Material science and characterization in advanced technology". Plasma heating experiments was performed with the support of the FFUG-2021-0001 project. Measurements of plasma parameters was performed with the support of the FFUG-2024-0028 project. Gyrokinetic simulation with the GENE code and power balance analysis using the ASTRA code was performed with the financial support of RSF, project No. 24-12-00162.

REFERENCES

[1]. S.M. Kaye, J, Plasma Phys. Control. Fusion, 63, 123001 (2021)
[2]. A.A. Galeev, R.Z. Sagdeev, Adv. Plasma Phys., 6, 311 (1976)
[3]. G.S. Kurskiev, Nucl. Fusion, 62, 104002 (2022)
[4]. S.A.M. McNamara, Nucl. Fusion, 63, 054002 (2023)

[5]. S.M. Kaye, Plasma Phys. Control. Fusion, 65, 095012 (2023)
[6]. Курскиев Г. С. Письма в ЖТФ, 2025, том 51, вып. 7
[7]. W. Tang, Nucl. Fusion 18, 1089 (1978)
[8]. B. Coppi and F. Pegoraro, Nucl. Fusion 17, 969 (1977)
[9]. B. Kadomtsev and O. Pogutse, Nucl. Fusion 11, 67 (1971)
[10]. W. Tang, J. Connor, and R. Hastie, Nucl. Fusion 20, 1439 (1980)
[11]. R. D. Hazeltine and H. R. Strauss, Phys. Rev. Lett. 37, 102 (1976)
[12]. J. F. Drake, N. T. Gladd, C. S. Liu, and C. L. Chang, Phys. Rev. Lett. 44, 994 (1980)
[13]. W. Guttenfelder et al., Phys. Rev. Lett. 106, 155004 (2011)
[14]. Y. C. Lee, J. Q. Dong, P. N. Guzdar, and C. S. Liu, Physics of Fluids 30, 1331 (1987)
[15]. W. Dorland, F. Jenko, M. Kotschenreuther, and B., Phys. Rev. Lett. 85, 5579 (2000)
[16]. Pereverzev G., Yushmanov P.N. Max-Plank IPP Report 5/98, 2002
[17]. Phys. Plasmas, Vol. 7, No. 5, May 2000
[18]. R. Arbon, J. Candy, and E. A. Belli. Plasma Physics and Controlled Fusion, 63(1):012001, January 2021.
[19]. Physics of Plasmas (1994-present) 6, 4265 (1999);
[20]. Houlberg W. et al 1997 Phys. Plasmas 4 3230
[21]. F. Jenko, J. Plasma Fusion Res. SERIES 6, 11 (2004).
[22]. T. G¨orler and F. Jenko, Phys. Rev. Lett. 100, 185002 (2008).
[23]. T. G¨orler and F. Jenko, Physics of Plasmas 15, 102508 (2008).
[24]. R. E. Waltz, J. Candy and M. Fahey, Physics of Plasmas 14, 056116 (2007).
[25]. Phys. Plasmas 26, 092510 (2019)
[26]. Candy and M. Fahey, Physics of Plasmas 14, 056116 (2007) 47